Received: 22 November 2023 | Revised: 16 December 2023 | Accepted: 28 December 2023

DOI: 10.1002/pc.28112

RESEARCH ARTICLE

spe INSPIRING PLASTICS PROFESSIONALS Polymer COMPOSITES WILEY

Damage mechanisms in composite laminated shells subjected to multiple impacts at different points

L. M. Ferreira[1,2] | **C. A. C. P. Coelho**[3] | **P. N. B. Reis**[4]

[1]Grupo de Elasticidad y Resistencia de Materiales, Escuela Técnica Superior de Ingeniería, Universidad de Sevilla, Sevilla, Spain

[2]Escuela Politécnica Superior, Universidad de Sevilla, Sevilla, Spain

[3]Unidade Departamental de Engenharias, Escola Superior de Tecnologia de Abrantes, Instituto Politécnico de Tomar, Abrantes, Portugal

[4]Department of Mechanical Engineering, University of Coimbra, CEMMPRE, ARISE, Coimbra, Portugal

Correspondence
L. M. Ferreira, Grupo de Elasticidad y Resistencia de Materiales, Escuela Técnica Superior de Ingeniería, Universidad de Sevilla, Camino Descubrimientos, S/N, Sevilla 41092, Spain.
Email: lmarques@us.es

Funding information
FCT–Fundação para a Ciência e a Tecnologia, Grant/Award Numbers: LA/P/0112/2020, UIDB/00285/2020

Abstract

This study investigates the effect of damage interference resulting from impact loads on the mechanical response and impact fatigue life of E-glass/epoxy composite laminate shells. The analysis involves single impacts at different points to evaluate the impact strength's dependency on boundary conditions. Notably, there is a gradual reduction in both maximum impact force and absorbed energy beyond 10 mm from the centre, towards unconstrained edges, accompanied by an increase in displacement. Specifically, at a distance of 30 mm, the maximum force and absorbed energy register a decrease of 9.4% and 7.9%, respectively, while the displacement rises by 14.5%. The findings reveal that the damage severity decreases as the impact point is closer to the unconstrained edge of the specimen, which can be attributed to a stiffness reduction, which can reach up to 22%. Symmetrically induced pre-damages exhibit no discernible effect on the subsequent impact response. It is observed that beyond 10 mm from the shell's centre, the number of impacts required to reach puncture increases by 10.5% and 21.1% for distances of 20 and 30 mm, respectively. Furthermore, it is also found that alternating impacts between symmetrical points show no inclination towards a preferential point for puncture.

Highlights

- The single impact strength's dependents on the boundary conditions.
- Reduction in both maximum impact force and absorbed energy near the unconstrained edges.
- Damage severity decreases as the impact point is closer to the unconstrained edges.
- Symmetrically induced pre-damages have no discernible effect on the subsequent impact response.
- Alternating impacts between symmetrical points show no inclination towards a preferential point for puncture.

KEYWORDS

composite laminated shells, damage interference, damage mechanisms, impact response, mechanical testing

1 | INTRODUCTION

Leveraging fiber-reinforced composite laminates in high-performance engineering applications provides a multitude of benefits compared to conventional materials.[1,2] Fiber-reinforced composite laminates excel in high-performance engineering applications due to their exceptional strength-to-weight ratio, customizable mechanical properties, and resistance to corrosion. Comprising fibers like carbon or glass embedded in a matrix, these materials offer a lightweight alternative with considerable strength, allowing for tailored designs. The flexibility to create intricate shapes, anisotropic properties for optimized mechanical behavior, and attributes like corrosion resistance and electrical insulation make them invaluable in aerospace, automotive, and similar demanding sectors.[3–8] Furthermore, the use of these materials in such industries leads to significant savings in fuel consumption due to their high specific strength and stiffness. Low-velocity impacts are common during manufacturing, transportation, and in-service conditions, making it crucial to understand how composites respond to such incidents. These impact loads can result in visible damage, such as delamination, matrix cracking, or fiber breakage within the composite structure. Even if not immediately apparent, these damages can compromise the material's mechanical properties, potentially leading to reduced structural performance and, in extreme cases, catastrophic failure. For example, according to the literature, reductions of 16%–25% in tensile strength have been reported due to the degradation of the fiber/matrix interface and stress concentration promoted by delaminations.[9–12] In terms of compression, the strength decreases around 60% due to multiple delaminations that interact and propagate rapidly due to buckling loads.[13–17] Finally, flexural strength can be affected between 34% and 78%, depending on the position of the delamination along the thickness and the layering sequence (symmetrical or anti-symmetrical).[18,19] Therefore, studying the impact response of composite materials is essential for designing components that can withstand a range of operational conditions and ensuring their reliability and safety in practical applications.

In recent decades, extensive research has been conducted on the effects of multiple low-velocity impacts at a single position, primarily investigating the mechanical behavior of various composite materials. Notable studies include Khazaie et al.'s[20] examination of basalt, Kevlar, and basalt-Kevlar hybrid fiber-reinforced epoxy composites, revealing that Basalt/Epoxy composites had the highest damage tolerance in comparison with Kevlar and fibers hybrid/epoxy. Saleh et al.[21] explored the residual compressive strength of composite laminates with different fabric architectures after repeated low-velocity impacts. The study unveiled that, despite the absorbed energy being nearly identical, 3D woven architectures exhibited the least damage. Additionally, in the context of compression after impact, 3D woven composites showcased a progressive damage behavior, ultimately resulting in the highest residual strength. Another relevant study is presented by Atas et al.[22] in which the authors delved into the repetitive impact response exhibited by woven composite laminates featuring diverse thicknesses. The authors found a linear variation in the puncture threshold/energy concerning thickness for the selected composite plates. Additionally, they developed a power equation that establishes a connection between impact energy and the requisite number of successive impacts for puncture. This formulation facilitates the prediction of the number of impacts required for puncture under lower impact energies without the need for actual testing. In summary, these studies investigate the impact performance of polymer-based composites reinforced with diverse materials and various fabric types. The research delves into the composites' response under different impact conditions, including high-velocity impacts, low-velocity impacts, and scenarios involving repeated impacts.

It is also possible to find in literature studies which focus is to explore the mechanical characteristics, such as maximum impact force and displacement, absorbed/dissipated energy resulting from multiple low-velocity impacts. For example, Liu[23] introduced the ratio of absorbed energy to impact energy for monitoring damage accumulation during repeated impacts, while Belingardi et al.[24] incorporated normalized maximum displacement into the energy absorption ratio to characterize the damage state. While these studies have significantly contributed to the understanding of repeated low-velocity impacts, they predominantly focus on a single position at the centre of composite laminate panels. In reality, multi-impacts often occur at different positions with varying distances between them and are not limited to flat structures. Therefore, thorough research on damage interference resulting from impacts at different positions in curved composite shells is imperative due to the widespread application of such structures in aerospace, automotive, and marine industries. The curved geometry introduces complexities in stress distributions and damage propagation mechanisms, making it essential to comprehend the implications of impacts on structural integrity. Identifying critical areas prone to damage and understanding how such damage may interact across different regions is crucial for predicting failure modes and implementing effective mitigation strategies. This research not only aids in designing resilient structures but also contributes to the development of predictive models and simulation tools, enabling engineers to assess the structural response of curved composite

shells and enhance the overall safety and performance of these components in diverse engineering applications. However, based on the various studies available in the literature,[18,19,25–28] they essentially analyze the impact response of semi-cylindrical composite shells when impacted at the same point. Nevertheless, daily experience shows that in most situations composite structures suffer repeated impacts in different positions due, for example, to hailstorms or particle impacts (among others). In this case, it is essential to understand the interference of the damage caused by impacts in multiple positions, because the problem when considering multiple impacts concentrated in a single position is too exaggerated.[29] In this context, the present study aims to understand the complex dynamics of multiple impact and damage interference scenarios to, subsequently, explain their effect on the mechanical response and impact fatigue life of composite laminated shell structures. For this purpose, the laminated composite shells were subjected to low-velocity impacts, considering two impact positions at the same distance from the centre. The impact points were positioned at distances ranging from 0 to 60 mm, subjecting the specimens to alternating impacts of 5.2 J. The results obtained were then compared with those from a control specimen, with a single central impact point and therefore unaffected by any previous neighboring impact damage.

2 | MATERIALS AND EXPERIMENTAL PROCEDURE

Composite semicylindrical shells were produced using the vacuum-assisted resin transfer molding (VARTM) technique, employing a SR1500 epoxy resin with SD2503 hardener, supplied by Sicomin (Châteauneuf-les-Martigues, France). These shells were reinforced with bidirectional E-glass woven fabric, featuring a plain-weave pattern with 205 g/m^2, supplied by Porcher Industries German GMbH (Erbach, Germany). The manufacturing process involved the stacking of 9 layers to achieve a final average thickness of 1.72 ± 0.07 mm. The average fiber volume fraction, determined via the burn-off method, was found to be approximately 51%.

The curing procedure adhered strictly to the manufacturer's guidelines,[30] involving the exposure of specimens to a vacuum pressure of 0.8 bars continuously for 24 hours. Post-manufacturing, the system underwent a curing phase at ambient temperature, lasting for 15 days to guarantee thorough curing. Notice that the curing cycle for epoxy resins is crucial as it initiates a chemical reaction, leading to cross-linking and the formation of a solid, durable material with enhanced mechanical and thermal properties, allowing for controlled cure time, improved adhesion, and temperature resistance. Subsequently, the specimens were cut, with a length of 130 ± 1 mm, utilizing a diamond blade saw, and employing an appropriate speed to mitigate overheating and to prevent interlaminar damage (delamination). Figure 1A illustrates the specimen dimensions and the location of the 7 in-line impact points (A, B_1, C_1, D_1, B_2, C_2 and D_2).

Finally, the low-velocity impact tests were carried out at room temperature conditions and using an IMATEK-IM10 instrumented drop-weight testing machine. Adjusting the drop height modifies the impact energy, which is generated by gravity. A piezoelectric load cell that can collect 32,000 points is used to quantify the impact force and the deflection is obtained from double integration of the acceleration versus time curve. More information about the equipment and data acquisition system can be found in.[31,32] Employing a hemispherical impactor with a diameter of 10 mm and a mass of 2.826 kg, the experimental tests were performed with a controlled impact energy of 5.2 ± 0.1 J, correlating to an impact velocity of approximately 1.92 m/s. This specific velocity was chosen with the intention of causing visible damage to the specimens during the initial impact while avoiding any puncturing. Figure 1B depicts the testing setup, showing that the specimens were free supported on the curved edges and the straight edges bi-supported.

Note that point A is located in the geometric centre of the specimen, while points B_1, B_2, C_1, C_2, D_1, and D_2 are 10, 20, and 30 mm away from point A, respectively. As shown in Figure 1A, the subscripts 1 and 2 indicate the side of the impact points in relation to point A. These distances were selected based on previous studies carried out by the authors and in accordance with Liao et al.[29] In more detail, at point A, repeated impact loads are systematically applied until puncture occurs, while for the remaining positions ($B_{1,2}$, $C_{1,2}$ and $D_{1,2}$) the impact load was applied alternately between each side until puncture was achieved (e.g., B_1 first and B_2 second). In the latter case, the specimens had to be positioned on the support to ensure that the point of impact was perfectly below the impactor. In addition, visual inspections and photographs were taken during the test campaign, using the translucent properties of the material and intense backlighting. Notice that the collapse defined in this study by puncture (full perforation) is detected visually and is characterized by the complete passage of the impactor through the samples.

Additionally, to determine the static response of specimens, compression tests were carried out at the central impact point (A) using a universal testing machine Shimadzu AG-100. To ensure consistency, the same support and impactor utilized in the low-velocity impact tests were employed, with a controlled displacement rate of 3 mm/min.

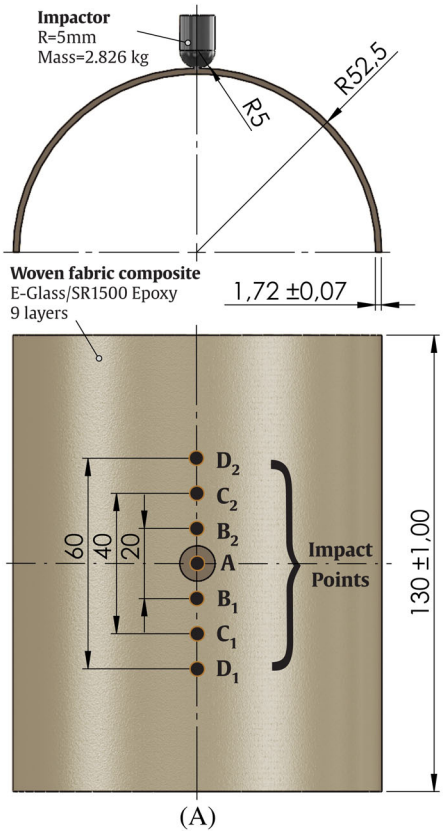

Instrumented drop-weight testing machine

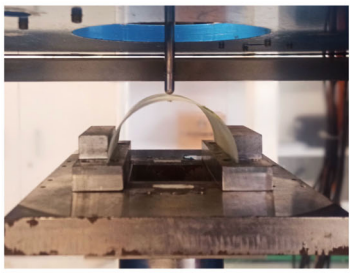

Specimen support device

(B)

FIGURE 1 Experimental setup: (A) Positioning of the 7 in-line impact points and dimensions of the tested specimens; (B) Drop-weight testing machine and specimen support device.

In total, 12 specimens were utilized for the low-velocity impact test, whole 3 were designated for the static compression tests. The distribution of the specimens for each test is summarized in Table 1. Despite the smaller sample size, the analysis provides valuable insights into the impact behavior of the materials under investigation. The use of state-of-the-art testing equipment contributed to the optimization of the information obtained from a limited number of samples and ensured consistent and relevant results within the given constraints. While acknowledging the potential limitations of a smaller sample size, the study aimed to maximize the available resources to contribute valuable data to the understanding of low-velocity impact characteristics in semicylindrical composite materials.

TABLE 1 Distribution of the specimens for the low-velocity impact tests and static compression tests.

	Number of tested specimens	
Set of impact points	**Low-velocity impact test**	**Static compression test**
A	3	3
$B_1 \mid B_2$	3	-
$C_1 \mid C_2$	3	-
$D_1 \mid D_2$	3	-

3 | RESULTS AND DISCUSSION

Initially, the influence of boundary conditions on impact strength was analyzed. Subsequently, these results will also be used to study the interference of damage caused by impacts in multiple positions. For this purpose, Figures 2 and 3 show the impact force time history and the energy time history, respectively, profiles that are very important because they provide qualitative information from the shape of the curves, as well as quantitative values that characterize some important parameters (maximum impact force, maximum displacement, contact time, and absorbed/restored energy).

These curves are representative of all the conditions tested, and are characterized by containing oscillations that can be attributed to the propagation of elastic waves, resulting from the specimen's vibrational response.[33,34] Furthermore, the curves show a profile that agrees with others reported in the literature for similar semicylindrical composite shells.[25–28,35,36] In more detail, Figure 2 shows an increase in the impact force until it reaches a maximum value, peak force, followed by a somewhat abrupt decrease, depending on the point of impact. Conversely, the energy-time curves represented

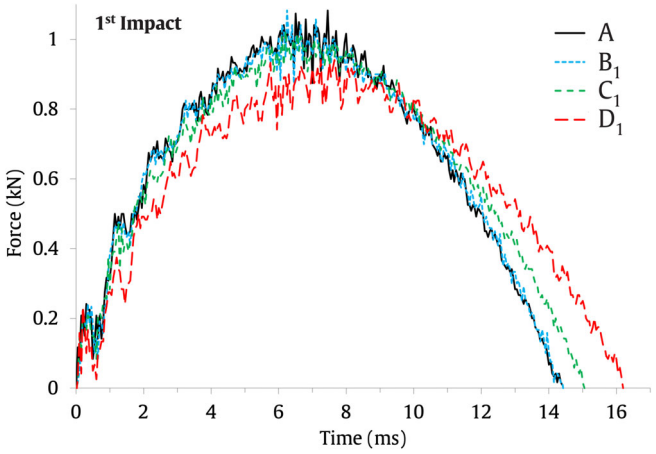

FIGURE 2 Force history curves obtained for the first impact at the various impact points.

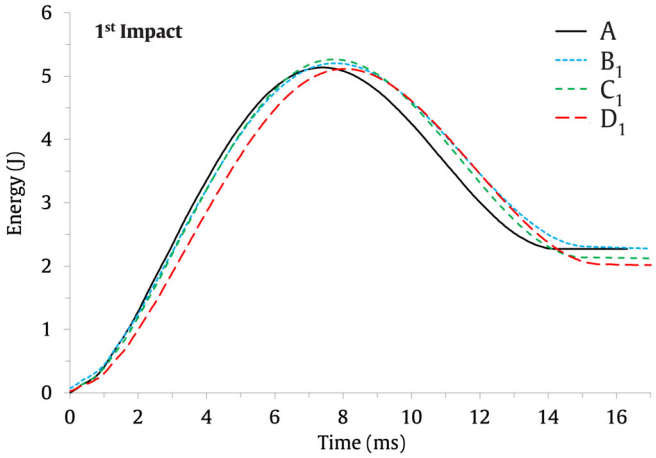

FIGURE 3 Energy history curves obtained for the first impact at the various impact points.

in Figure 3 reveal that the impact energy utilized during the tests does not attain sufficient magnitude to puncture the specimens. Instead, the impactor hits the specimens and returns by rebound. According to literature, the inception of the plateau phase corresponds to the point where contact between the impactor and the specimen is lost. Consequently, the component of restored energy (elastic component) is defined as the difference between the maximum energy and the energy evident during the plateau phase.[37–39]

From a numerical point of view, and based on these curves, it is possible to quantify the maximum force, maximum displacement, contact time and absorbed energy, parameters which are summarized in Figure 4. The values are presented in terms of average values, and to represent the inherent variability and uncertainties in the data, scatter bands were added. These bands illustrate the range of values obtained for each condition, showcasing both the maximum and minimum values.

It can be seen from Figure 4A that the magnitude of the average maximum force remains unchanged until a distance of 10 mm from point A, at which point the force begins to decrease. For example, compared to the value obtained at point A, the maximum force decreases by 8.5% and 9.4% when the impact occurs at points C_1 (20 mm) and D_1 (30 mm), respectively. In terms of maximum displacement, a similar behavior is observed, but in this case the magnitude of the displacement increases, as the impact point moves towards the edge of the shell (unconstrained edge). Compared to point A, the maximum displacement increases by around 9.2% at point C_1 and by 14.5% at point D_1. Regarding contact time and absorbed energy, Figure 4B shows that in the first case the evolution of contact time is aligned with the maximum displacement, while the absorbed energy mirrors what is observed for the maximum force. For points C_1 and D_1, the contact time increases by around 8.3% and 11.8%, while the absorbed energy decreases about 4.3% and 7.9%, respectively, when the values are compared with those obtained for point A. It should be noted that the information regarding contact time supplements other impact parameters such as force, displacement, energy absorption, and impact bending stiffness. It holds relevance for subsequent numerical studies, playing a key role in refining numerical models to establish a numerical-experimental correlation. This correlation is essential for validating the developed model in the context of the specific topic under investigation.

The changes described above for the maximum impact force, maximum displacement, contact time and absorbed energy are justified by the stiffness gradient observed when the impact point moves towards the edge.[39,40] According to Minak and Ghelli,[40] stiffer components tend to suffer more extensive damage due to their limited capacity to store elastic energy before failure. On the other hand, they observed that lower stiffness facilitates higher displacements and lower energy absorptions, which is in line with what is observed in Figure 4B. Moreover, to complement this analysis, Figure 5 shows the damage suffered at the various impact points, revealing a decrease in the severity of the damage as the impact point moves away from the centre and closer to the edge of the shell. Notice that the dimension depicted in each detailed view corresponds to the distance between two adjacent impact points, facilitating the assessment of the extent of the introduced damage.

Finally, to prove the validity of the analysis presented, a static numerical study was performed using 3D finite element (FE) models. These FE models were developed based on the approach and material properties outlined in,[25,27,28] along with the geometric parameters of the impactor and composite shell specimens depicted in Figure 1. Additionally, the boundary conditions imposed

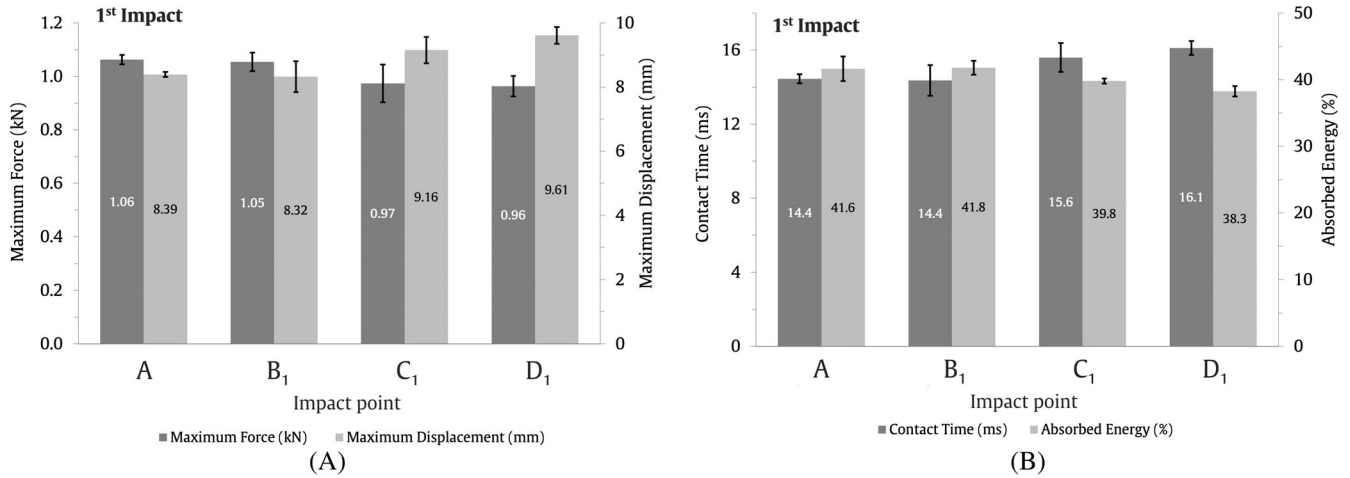

FIGURE 4 Effect of the impact location for the first impact in terms of: (A) maximum impact force, displacement; (B) contact time and absorbed energy.

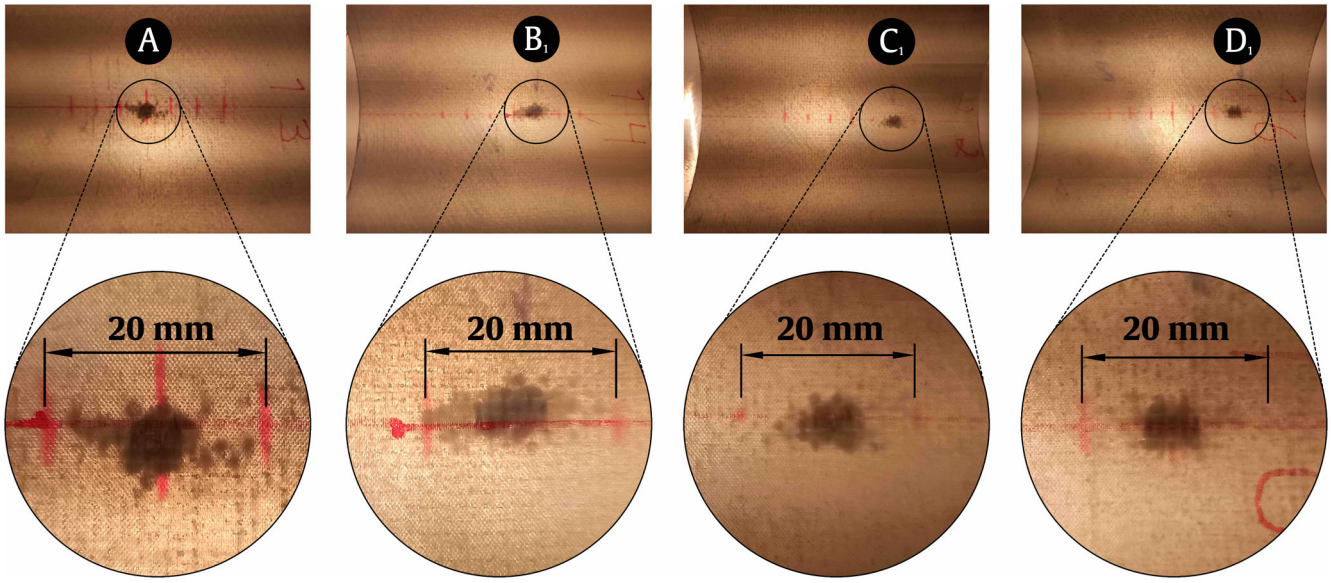

FIGURE 5 Damage observed for the first impact at impact points A, B_1, C_1 and D_1.

were defined according to the experimental testing setup represented in Figure 1B. The 9 woven fabric laminas were modeled as a linear elastic homogeneous material, considering their transversely isotropic behavior. The progressive damage was incorporated using the ABAQUS/Standard built-in damage initiation criteria for fiber-reinforced composite materials.[41,42] Furthermore, the damage evolution response was defined based on the energy dissipation during the damage process. Continuum shell elements with eight nodes and reduced integration (SC8R) were employed. The nonlinear effects of large deformations and displacements were accounted for. The FE mesh discretization is shown in Figure 6A, comprising of approximately 65.000 elements and 80.000 nodes.

To verify the reliability of the numerical predictions, a comparison with the force-displacement results from experimental static compressive tests conducted at the impact point A was undertaken. A good numerical-experimental correlation was attained as evident in Figure 6A. Subsequently, the numerical predictions for all other impact points are showcased in Figure 6B. For ease of comparison, the numerically predicted stiffness values at the various impact points are listed in Table 2. Notice that, owing to the symmetry of both the FE model and the impact points, the numerical results are identical on both sides; for instance, B_1 equals B_2. Consequently, they are denoted only as points B, C, and D, in Figure 6, as well as in Table 2.

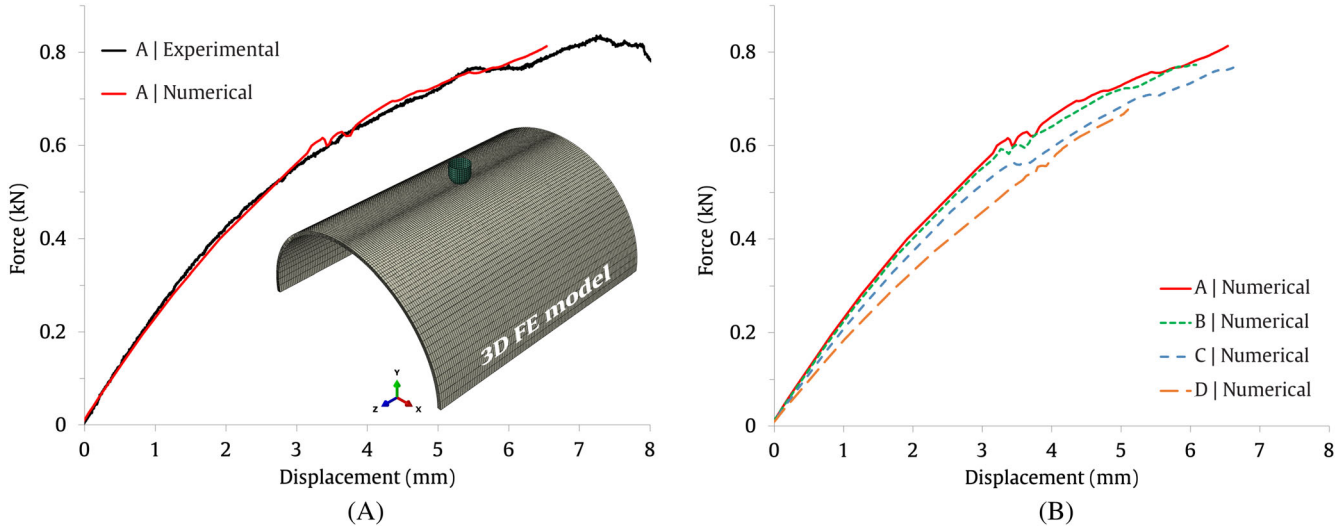

FIGURE 6 Force-displacement curves obtained from static compressive tests: (A) Experimental and numerical predictions at impact point A; (B) Numerical predictions at the impact points A, B, C and D.

TABLE 2 Numerically predicted stiffnesses at impact points A, B, C and D and percent change from point A.

Impact point	Stiffness (kN/mm)	Percent change
A	0.241	-
B	0.232	−3.7%
C	0.214	−11.2%
D	0.188	−22%

It becomes apparent that the force-displacement curves obtained at the impact points A and B exhibit considerable similarity throughout the analysis. However, a noteworthy trend emerges: the closer the impact point is to the edge of the shell (unconstrained edge), the greater the reduction in stiffness. The impact point B_1 demonstrates a 3.7% reduction in stiffness compared to impact point A, whereas impact points C and D manifest more substantial reductions, with stiffness values 11.2% and 22% lower, respectively. Therefore, because the boundary conditions imposed in the FE model were kept unchanged for all the impact points, these results can be attributed to the greater allowance for deformation and rotation as the impact point approaches the free edge of the shell. This evidence reaffirms the analyses previously conducted on the single impact response at various impact points, in which the different stiffness values explain the lower damage observed.

After the analysis of the impact point effect, this study also focuses on the existence of a pre-damage (B_1, C_1 or D_1) caused symmetrically and at the same distance from the current impact (B_2, C_2 or D_2), as shown in Figure 1A. For this purpose, Figure 7 compares the average values obtained for the maximum force, maximum displacement, contact time and absorbed energy, parameters that were used as a first step to highlight the effect of the distance between the impact point and the pre-damage caused by a load applied under the same conditions.

It can be observed that all the parameters (maximum force, maximum displacement, contact time and absorbed energy) analyzed evolve according to the same behavior described above, that is, the maximum force and absorbed energy decrease when the impacts are closer to the free edges of the shell, while the maximum displacement and contact time increase. Furthermore, the difference between values does not reveal any effect of the pre-damages (B_1, C_1 and D_1), because the greatest difference (around 3.2%) occurred for the maximum displacement between points B_1 and B_2, but without statistical significance due to the dispersion observed. In this context, it can be concluded that, for the dimensions between the impact points studied, there is no effect of the pre-damage on the impact parameters analyzed, that is, the pre-damage introduced did not affect the stiffness of the current impact point. Although some studies available in the literature report that pre-damage no longer influences the impact strength for distances greater than 20 mm,[39,43,44] these do not contradict the results of this study because they were obtained for flat plates. According to Zhao and Cho,[45] the damage size is related to the total dynamic deformation and the damage size of these structures is smaller than that observed in flat plates, as well as its position changes from the lower interface to the upper interface.[46] Finally, to complement this analysis, Figure 8 shows the damage observed for the different impact points, B_2, C_2 and D_2, as a function of the pre-damage

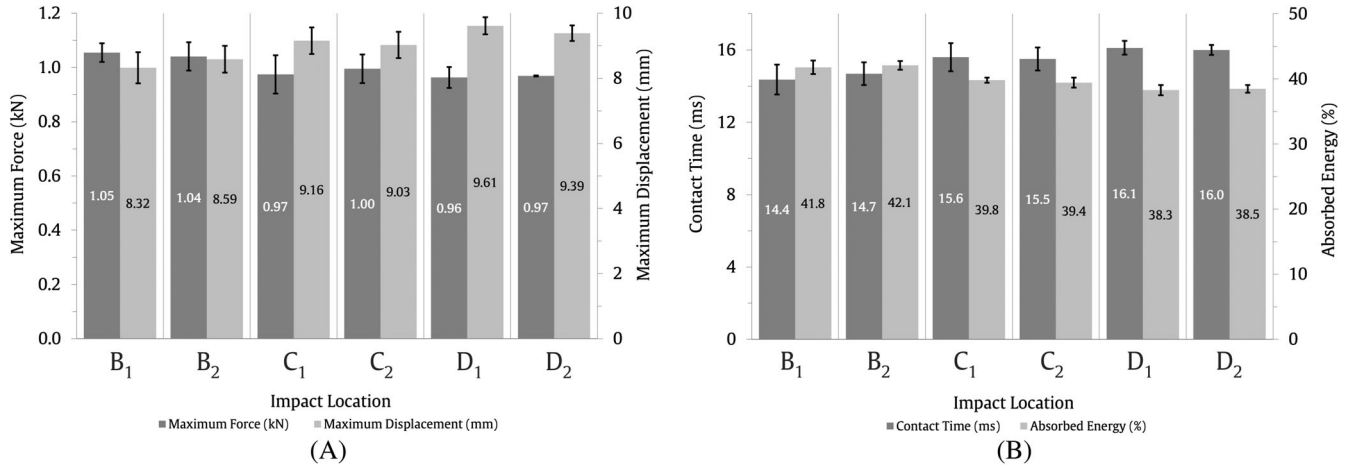

FIGURE 7 Effect of the distance between the impact point and a pre-damage located symmetrically and at the same distance from the current impact in terms of: (A) maximum impact force, displacement; (B) contact time and absorbed energy.

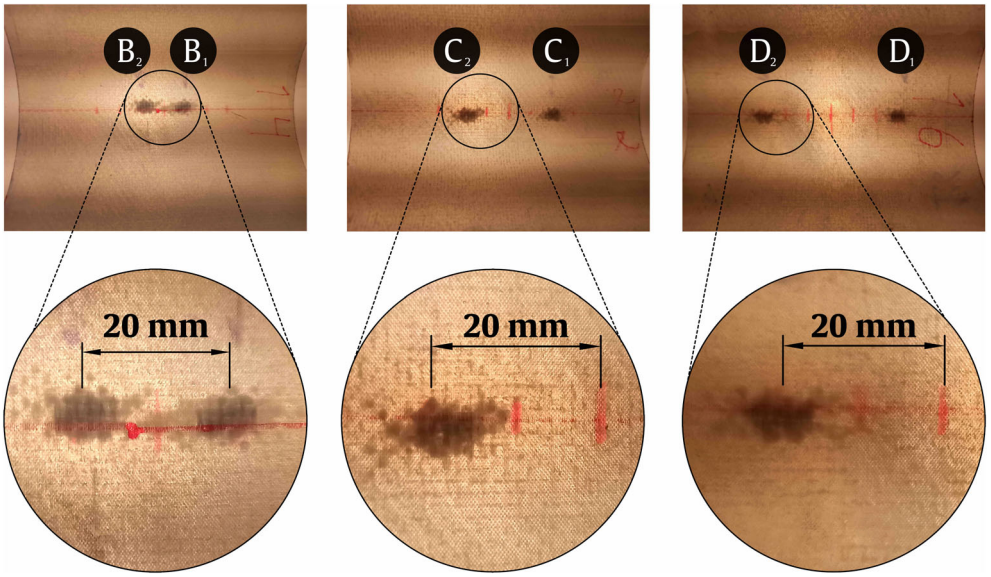

FIGURE 8 Effect of pre-damages (B_1, C_1 and D_1) on the impact strength for different impact points (B_2, C_2 and D_2).

located at B_1, C_1 and D_1. As can be seen, the damage dimensions at B_2, C_2 and D_2 are very similar to those observed at B_1, C_1 and D_1, denoting that, for the distances studied, the pre-damage does not intersect with the current damage nor affects the stiffness of the impact points at B_2, C_2 and D_2.

On the other hand, literature also reports that the damage can be correlated with the impact bending stiffness (IBS), a parameter that is obtained by the slope of the upward section of the force-displacement curve.[47–49] In this context, given the similarity of the damage observed for each impact point analyzed, similar values of IBS are expected. Therefore, to validate this hypothesis, Table 3 presents the various IBS values, confirming that, in fact, the values are very similar for each considered impact point. Furthermore, this table also corroborates the numerical predictions presented in Table 2, where the IBS values also decrease as the edge approaches and, consequently, smaller damages are obtained (as shown in Figure 8).

TABLE 3 Impact bending stiffness values for each impact point, and percent change from point A.

Impact point	IBS (kN/mm)	Percent change
A	0.160 ± 0.01	-
B_1 | B_2	0.157 ± 0.02 | 0.157 ± 0.01	−1.9% | −1.9%
C_1 | C_2	0.149 ± 0.02 | 0.150 ± 0.02	−6.9% | −6.3%
D_1 | D_2	0.135 ± 0.03 | 0.137 ± 0.02	−15.6% | −14.4%

Finally, the multi-impact effect was also analyzed, and the results obtained are shown in Figure 9. The white symbols represent the first impact, while the black ones represent the second impact, that is, the impact after

a pre-damage introduced by the first impact. For comparison purposes, the multi-impact occurring at the same point (A) was also included.

From Figure 9 it is possible to conclude that up to a distance of 10 mm from point A, the impact fatigue life remains unchanged, but, for higher values, a slight increase in the number of impacts to reach puncture is observed. Quantifying this trend, the number of impacts necessary to achieve puncture varied between 16 and 23 impacts, whose average value is around 19 impacts, and is characterized by all impacts occurring at the same point (central position A). For position B, the average impact fatigue life is the same, which shows that the damage introduced interacts with each other, due to the proximity of the impact points, and providing a situation very similar to that which occurred for central position A (damage superimposed by superimposed impacts). In fact, the evidence shown in Figure 8 already indicated this. Subsequently, compared to these values, the number of impacts to achieve full perforation increases by around 10.5% and 21.1% for the impact positions C and D, respectively. Furthermore, because the impacts alternated between two symmetrical points, no preferential point for perforation to occur was observed.

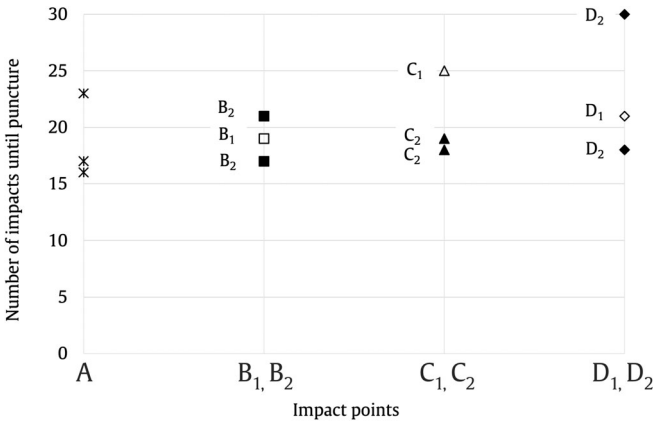

FIGURE 9 Number of impacts until full perforation versus impact point.

Figure 10 corroborates the analysis described above, showing the evolution of damage with the number of impacts. For all situations, it is noticed that the severity of the damage increases with the number of impacts, but with particular severity for the impact points B_1 and B_2. In this case, the damage overlapping is clearly visible, which justifies an average impact fatigue life similar to that obtained for point A. Therefore, due to this damage accumulation, the maximum impact force decreases, and the maximum displacement increases.[48,50–52]

This evidence is corroborated by Figure 11, which shows various force-displacement curves for successive impacts at points B_1 and B_2. However, they are representative of all the conditions studied and, from the results obtained, it was possible to observe that the maximum impact force decreased between 25% and 30%, while the maximum displacement increased between 45% and 65%. Furthermore, the accumulation of damage reduces the stiffness, especially at the point of impact[48,51] and, although there is no law correlating these parameters,

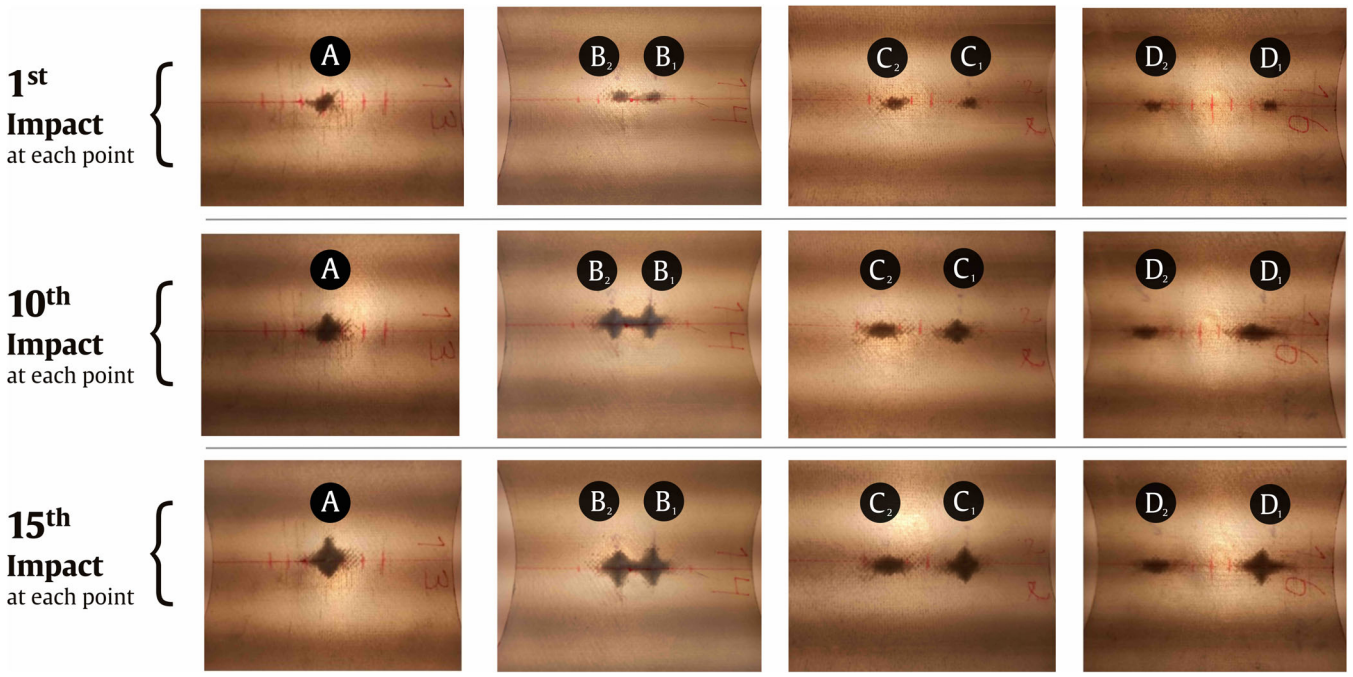

FIGURE 10 Damage evolution for the different impact points.

Figure 11 clearly shows the existence of a dependency between impact force, displacement and stiffness. On the other hand, the slope of the upward sections of the force-displacement curves illustrated in Figure 11 shows that the IBS decreases with the number of impacts and corroborates all the previous discussion.

Finally, when Figures 10 and 11 are analyzed together, it can be concluded that increasing the number of impacts increases the severity of the damage while the IBS decreases. These findings are in line with studies developed by Amaro et al.,[53,54] in which the damage severity is inversely related with IBS and directly related to the amount of energy absorbed. Therefore, lower IBS values are associated with higher absorbed energy values, and this evidence can be confirmed by analyzing Figures 11 and 12 together. Figure 12 shows typical energy versus time curves for impact points B_1 and B_2, but they are representative of all conditions studied. From the curves shown, it can be noticed that the restored/elastic energy decreases with the number of impacts, which means that more energy is absorbed by the specimen and, consequently, corresponds to a greater damage accumulation and lower stiffness. Therefore, this evidence once again proves what was reported above.

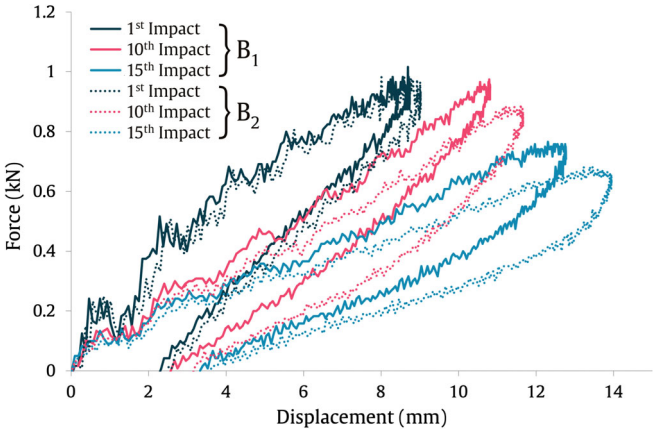

FIGURE 11 Representative impact response in terms of force versus displacement curves.

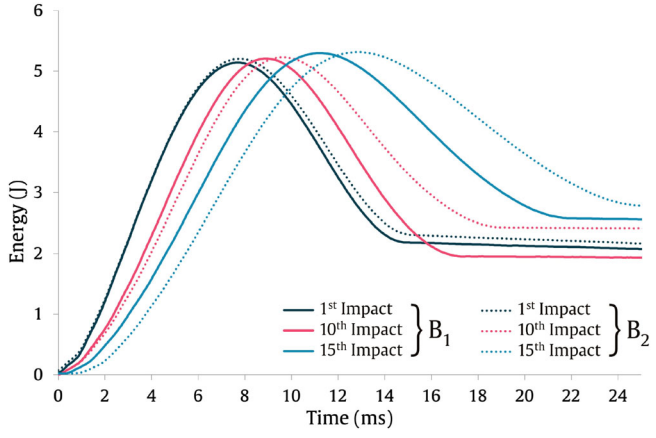

FIGURE 12 Representative impact response in terms of energy versus time curves.

4 | CONCLUSIONS

The aim of this study was to evaluate the effect of pre-damage (damage interference) obtained by impact loads on the impact fatigue live of E-glass/epoxy cylindrical composite laminate shells.

Initially, single impacts at different impact points were considered to assess the influence of boundary conditions on the impact strength. It was observed that the maximum impact force and absorbed energy progressively decreased for distances greater than 10 mm from the center and in the direction of the unconstrained edges of the specimen, while the maximum displacement increased. For example, for a distance of 30 mm from the center of the specimen, the maximum force and absorbed energy decreased by 9.4% and 7.9%, respectively, compared to the values obtained for the impact in the center of the specimen, while the displacement increased by 14.5%. Consequently, the size of the damage also decreased. This was explained by the reduction in stiffness, where a decrease of around 22% was observed between the impact points considered above (0 and 30 mm).

In terms of the effect of the pre-damages caused symmetrically and at the same distance from the current impact, no effect was observed on the impact parameters analyzed, which means that the induced pre-damage did not affect the stiffness of the recent impact point. Finally, it was also observed that there is no effect of the impact point on the impact fatigue life up to 10 mm from the center point, after which there is a slight increase in the number of impacts (10.5% for 20 mm and 21.1% for 30 mm) to reach full perforation. Furthermore, because the impacts alternated between two symmetrical points, there was no preferential point where the perforation occurred.

Therefore, in real multiple impact scenarios, it is impossible to guarantee minimum distances to avoid damage interference. This is even more difficult when impacts are too frequent, such as in hailstorms or aircraft landing/take-off. In this context, based on current knowledge and despite being a very conservative design approach, it is much safer when the multiple impacts concentrated in a single position are considered.

ACKNOWLEDGMENTS

This research was sponsored by national funds through FCT–Fundação para a Ciência e a Tecnologia, under the project UIDB/00285/2020 and LA/P/0112/2020.

DATA AVAILABILITY STATEMENT

The data that support the findings of this study are available from the corresponding author upon reasonable request.

ORCID

L. M. Ferreira https://orcid.org/0000-0002-5223-5309

REFERENCES

1. Chen S, Hu J, Han S, Guo Y, Belzile N, Deng T. A review on emerging composite materials for cesium adsorption and environmental remediation on the latest decade. *Sep Purif Technol*. 2020;251:117340. doi:10.1016/j.seppur.2020.117340
2. Tornero RG. Composite materials are more present today than ever before in cars. *Reinf Plast*. 2015;59:131. doi:10.1016/j.repl.2015.01.004
3. Le Lay F, Gutierrez J. Improvement of the fire behaviour of composite materials for naval application. *Polym Degrad Stab*. 1999;64:397-401. doi:10.1016/S0141-3910(98)00140-2
4. Fantuzzi N, Bacciocchi M, Benedetti D, Agnelli J. The use of sustainable composites for the manufacturing of electric cars. *Compos Part C Open Acc*. 2021;4:100096. doi:10.1016/j.jcomc.2020.100096
5. Kelkar AD, Tate JS, Chaphalkar P. Performance evaluation of VARTM manufactured textile composites for the aerospace and defense applications. *Mater Sci Eng B Solid-State Mater Adv Technol*. 2006;132:126-128. doi:10.1016/j.mseb.2006.02.034
6. Ferreira L, Coelho C. Modelling progressive damage in NCF composites using the continuum damage mechanics method. *2022 Advances in Science and Engineering Technology International Conferences (ASET)*. IEEE; 2022:1-4. doi:10.1109/ASET53988.2022.9734944
7. Ferreira LM, Graciani E, París F. Three dimensional finite element study of the behaviour and failure mechanism of non-crimp fabric composites under in-plane compression. *Compos Struct*. 2016;149:106-113.
8. Ferreira LM, Graciani E, París F. Predicting failure load of a non-crimp fabric composite by means of a 3D finite element model including progressive damage. *Compos Struct*. 2019;225:111115. doi:10.1016/j.compstruct.2019.111115
9. Reis PNB, Ferreira JAM, Antunes FV, Richardson MOW. Effect of interlayer delamination on mechanical behavior of carbon/epoxy laminates. *J Compos Mater*. 2009;43:2609-2621. doi:10.1177/0021998309344649
10. Mosallam A, Slenk J, Kreiner J. Assessment of residual tensile strength of carbon/epoxy composites subjected to low-energy impact. *J Aerosp Eng*. 2008;21:249-258. doi:10.1061/(ASCE)0893-1321(2008)21:4(249)
11. Mittelman A, Roman I. Tensile properties of real unidirectional Kevlar/epoxy composites. *Composites*. 1990;21:63-69. doi:10.1016/0010-4361(90)90099-I
12. Obrien T, Rigamonti M, Zanotti C. Tension fatigue analysis and life prediction for composite laminates. *Int J Fatigue*. 1989;11:379-393. doi:10.1016/0142-1123(89)90177-1
13. Zheng S, Sun CT. Delamination interaction in laminated structures. *Eng Fract Mech*. 1998;59:225-240. doi:10.1016/S0013-7944(97)00120-3
14. De Moura M, Marques A. Prediction of low velocity impact damage in carbon–epoxy laminates. *Compos A: Appl Sci Manuf*. 2002;33:361-368.
15. Suemasu H, Sasaki W, Ishikawa T, Aoki Y. A numerical study on compressive behavior of composite plates with multiple circular delaminations considering delamination propagation. *Compos Sci Technol*. 2008;68:2562-2567. doi:10.1016/j.compscitech.2008.05.014
16. Lee S-Y, Park D-Y. Buckling analysis of laminated composite plates containing delaminations using the enhanced assumed strain solid element. *Int J Solids Struct*. 2007;44:8006-8027. doi:10.1016/j.ijsolstr.2007.05.023
17. Amaro AM, Reis PNB, De Moura MFSF, Neto MA. Buckling analysis of laminated composite plates submitted to compression after impact. *Fibers Polym*. 2014;15:560-565. doi:10.1007/s12221-014-0560-x
18. Amaro AM, Reis PNB, De Moura MFSF. Residual strength after low velocity impact in carbon-epoxy laminates. *MSF*. 2006;514–516:624. doi:10.4028/MSF.514-516.624
19. Amaro AM, Reis PNB, De Moura MFSF. Delamination effect on bending behaviour in carbon-epoxy composites: bending behaviour in carbon-epoxy composites. *Strain*. 2011;47:203-208. doi:10.1111/j.1475-1305.2008.00520.x
20. Khazaie M, Eslami-Farsani R, Saeedi A. Evaluation of repeated high velocity impact on polymer-based composites reinforced with basalt and Kevlar fibers. *Mater Today Commun*. 2018;17:76-81. doi:10.1016/j.mtcomm.2018.08.016
21. Saleh MN, El-Dessouky HM, Saeedifar M, De Freitas ST, Scaife RJ, Zarouchas D. Compression after multiple low velocity impacts of NCF, 2D and 3D woven composites. *Compos A: Appl Sci Manuf*. 2019;125:105576. doi:10.1016/j.compositesa.2019.105576
22. Atas C, Icten BM, Küçük M. Thickness effect on repeated impact response of woven fabric composite plates. *Compos Part B Eng*. 2013;49:80-85. doi:10.1016/j.compositesb.2013.01.019
23. Liu D. Characterization of impact properties and damage process of glass/epoxy composite laminates. *J Compos Mater*. 2004;38:1425-1442. doi:10.1177/0021998304042741
24. Belingardi G, Cavatorta MP, Paolino DS. A new damage index to monitor the range of the penetration process in thick laminates. *Compos Sci Technol*. 2008;68:2646-2652. doi:10.1016/j.compscitech.2008.04.029
25. Ferreira LM, Coelho CACP, Reis PNB. Numerical predictions of intralaminar and interlaminar damage in thin composite shells subjected to impact loads. *Thin-Walled Struct*. 2023;192:111148. doi:10.1016/j.tws.2023.111148
26. Ferreira L, Coelho C, Reis P. Impact response of semi-cylindrical composite laminate shells under repeated low-velocity impacts. *Adv Sci Eng Technol Int Conf (ASET)*. 2022;2022:1-5. doi:10.1109/ASET53988.2022.9735043
27. Ferreira LM, Coelho CACP, Reis PNB. Effect of cohesive properties on low-velocity impact simulations of woven composite shells. *Appl Sci*. 2023;13:6948. doi:10.3390/app13126948
28. Ferreira LM, Coelho CACP, Reis PNB. Numerical simulations of the low-velocity impact response of semicylindrical woven composite shells. *Materials*. 2023;16(9):3442. doi:10.3390/ma16093442
29. Liao B, Wang P, Zheng J, et al. Effect of double impact positions on the low velocity impact behaviors and damage interference mechanism for composite laminates. *Compos A: Appl Sci Manuf*. 2020;136:105964. doi:10.1016/j.compositesa.2020.105964
30. S. E. Systems. Sicomin Technical Datasheet. 2014.
31. Ferreira LM, Aranda MT, Muñoz-Reja M, Coelho C, Távara L. Ageing effect on the low-velocity impact response of 3D printed

continuous fibre reinforced composites. *Compos Part B Eng*. 2023;267:111031. doi:10.1016/j.compositesb.2023.111031
32. Amaro AM, Reis PNB, Magalhães AG, de Moura MFSF. The influence of the boundary conditions on low-velocity impact composite damage. *Strain*. 2011;47:e220-e226. doi:10.1111/j.1475-1305.2008.00534.x
33. Schoeppner GA, Abrate S. Delamination threshold loads for low velocity impact on composite laminates. *Compos A: Appl Sci Manuf*. 2000;31:903-915.
34. Belingardi G, Vadori R. Low velocity impact tests of laminate glass-fiber-epoxy matrix composite material plates. *Int J Impact Eng*. 2002;27:213-229.
35. Reis PNB, Coelho CACP, Navalho FVP. Impact response of composite Sandwich cylindrical shells. *Appl Sci*. 2021;11:11. doi:10.3390/app112210958
36. Campos Pais Coelho CA, Navalho FVP, Reis PNB. Impact response of laminated cylindrical shells. *Fra&IntStrut*. 2019;13:411-418. doi:10.3221/IGF-ESIS.48.39
37. Gómez-del Río T, Zaera R, Barbero E, Navarro C. Damage in CFRPs due to low velocity impact at low temperature. *Compos Part B Eng*. 2005;36:41-50. doi:10.1016/j.compositesb.2004.04.003
38. Reis P, Santos P, Ferreira J, Richardson M. Impact response of sandwich composites with nano-enhanced epoxy resin. *J Reinf Plast Compos*. 2013;32:898-906. doi:10.1177/0731684413478993
39. Amaro AM, Reis PNB, de Moura MFSF, Neto MA. Influence of open holes on composites delamination induced by low velocity impact loads. *Compos Struct*. 2013;97:239-244. doi:10.1016/j.compstruct.2012.09.041
40. Minak G, Ghelli D. Influence of diameter and boundary conditions on low velocity impact response of CFRP circular laminated plates. *Compos Part B Eng*. 2008;39:962-972. doi:10.1016/j.compositesb.2008.01.001
41. Dassault Systemes. ABAQUS n.d.
42. Hashin Z. Failure criteria for unidirectional fiber composites. *J Appl Mech*. 1980;47:329-334. doi:10.1115/1.3153664
43. Santos RAM, Reis PNB, Santos MJ, Coelho CACP. Effect of distance between impact point and hole position on the impact fatigue strength of composite laminates. *Compos Struct*. 2017;168:33-39. doi:10.1016/j.compstruct.2017.02.045
44. Reis PNB, Santos RAM, Silva FGA, De Moura MFSF. Influence of hole distance on low velocity impact damage. *Fibers Polym*. 2018;19:2574-2580. doi:10.1007/s12221-018-8376-8
45. Zhao GP, Cho CD. Damage initiation and propagation in composite shells subjected to impact. *Compos Struct*. 2007;78:91-100. doi:10.1016/j.compstruct.2005.08.013
46. Cho C, Zhao G. Dynamic response and damage of composite shell under impact. *KSME Int J*. 1999;13:596-608.
47. David-West O, Nash D, Banks W. An experimental study of damage accumulation in balanced CFRP laminates due to repeated impact. *Compos Struct*. 2008;83:247-258.
48. Amaro AM, Reis PNB, Neto MA. Experimental study of temperature effects on composite laminates subjected to multi-impacts. *Compos Part B Eng*. 2016;98:23-29. doi:10.1016/j.compositesb.2016.05.021
49. Reis PNB, Sousa P, Ferreira LM, Coelho CACP. Multi-impact response of semicylindrical composite laminated shells with different thicknesses. *Compos Struct*. 2023;310:116771. doi:10.1016/j.compstruct.2023.116771
50. Amaro AM, Reis PNB, de Moura MFSF, Neto MA. Multi-impact response of composite laminates with open holes. *Polym Compos*. 2018;39:2490-2498. doi:10.1002/pc.24235
51. Coelho SRM, Reis PNB, Ferreira JAM, Pereira AM. Effects of external patch configuration on repaired composite laminates subjected to multi-impacts. *Compos Struct*. 2017;168:259-265. doi:10.1016/j.compstruct.2017.02.069
52. Azouaoui K, Rechak S, Azari Z, Benmedakhene S, Laksimi A, Pluvinage G. Modelling of damage and failure of glass/epoxy composite plates subject to impact fatigue. *Int J Fatigue*. 2001;23:877-885. doi:10.1016/S0142-1123(01)00050-0
53. Amaro A, Reis P, Neto M, Louro C. Effects of alkaline and acid solutions on glass/epoxy composites. *Polym Degrad Stab*. 2013;98:853-862.
54. Amaro A, Reis P, Neto M, Louro C. Effect of different acid solutions on glass/epoxy composites. *J Reinf Plast Compos*. 2013;32:1018-1029. doi:10.1177/0731684413483886

How to cite this article: Ferreira LM, Coelho CACP, Reis PNB. Damage mechanisms in composite laminated shells subjected to multiple impacts at different points. *Polym Compos*. 2024; 1-12. doi:10.1002/pc.28112